

The extended pulsar magnetosphere

Constantinos Kalapotharakos,^{1,2*} Ioannis Contopoulos^{3*} and Demos Kazanas^{2*}

¹University of Maryland, College Park (UMDCP/CRESST), College Park, MD 20742, USA

²Astrophysics Science Division, NASA/Goddard Space Flight Center, Greenbelt, MD 20771, USA

³Research Center for Astronomy and Applied Mathematics, Academy of Athens, Athens 11527, Greece

Accepted 2011 September 23. Received 2011 September 22; in original form 2011 June 5

ABSTRACT

We present the structure of the 3D ideal magnetohydrodynamics pulsar magnetosphere to a radius 10 times that of the light cylinder, a distance about an order of magnitude larger than any previous such numerical treatment. Its overall structure exhibits a stable, smooth, well-defined undulating current sheet which approaches the kinematic split monopole solution of Bogovalov only after a careful introduction of diffusivity even in the highest resolution simulations. It also exhibits an intriguing spiral region at the crossing of two zero-charge surfaces on the current sheet, which shows a destabilizing behaviour more prominent in higher resolution simulations. We discuss the possibility that this region is physically (and not numerically) unstable. Finally, we present the spiral pulsar antenna radiation pattern.

Key words: magnetic fields – MHD – radiation mechanisms: general – methods: numerical – pulsars: general.

1 INTRODUCTION

Almost half a century since the discovery of pulsars and despite the great observational progress, a comprehensive understanding of the observed radiation remains elusive. This is to a large extent due to its breadth in frequency (from radio to gamma-rays) and dependence on the pulsar rotation phase as well as on its potential dependence on the (unknown) observer inclination angle and the angle between the rotation and magnetic axes.

Pulsar radio emission remains the hardest to model (mainly because of its apparently coherent character) and most models that claim to account for its main features (multiple pulse profiles, polarization angle sweeps, pulse width–wavelength relation, etc.) are simply phenomenological. It is considered that radio emission originates in (probably hollow) conical beams above the magnetic polar caps. The situation is slightly better at higher energies (optical to gamma-rays) where the recent *Fermi* observations indicate the emission region to be associated with the outer magnetosphere even beyond the light cylinder (Ransom et al. 2011; Guillemot et al. 2011). The exact emission mechanism remains unclear; however, it is generally considered to be curvature radiation emitted by relativistic electrons moving along the pulsar magnetic field lines near the separatrix between the closed and open field lines, although synchrotron and inverse-Compton emission could potentially make important contributions to the spectrum (Muslimov & Harding 2004; Harding et al. 2008).

Given the relativistic unidirectional motion of the pulsar radiating particles, any significant advance in understanding their emission across the electromagnetic spectrum must take into account the detailed structure of the pulsar magnetosphere. Its structure, even in the axisymmetric, aligned dipole field, had been unknown until rather recently. Following the original solution of Contopoulos, Kazanas & Fendt (1999), a number of additional treatments have established the precise structure of this configuration (Contopoulos 2005; Gruzinov 2005; Timokhin 2006). More recently, the structure of the non-aligned dipole was obtained numerically (Spitkovsky 2006; Kalapotharakos & Contopoulos 2009); this was then used to produce kinematic model light curves by placing the emission of radiation both near to (Bai & Spitkovsky 2010) and well outside the light cylinder (Contopoulos & Kalapotharakos 2010), with results that apparently are both consistent with observations. The idea that the observed radiation is sited outside the light cylinder was not new. Lyubarsky (1996) had proposed the possibility that the high-energy emission comes from sites just beyond the light cylinder at the reconnection region near the Y-point, while Pétri & Kirk (2005) proposed the stripped wind model in which the observed radiation comes from a zone far beyond the light cylinder.

The most recent multifrequency observations of pulsar emission do not seem to provide a preference between these rather diverse sites of pulsar emission, being in general phenomenological agreement with both. In fact, in most pulsars with both gamma-ray and radio observations available (56 as of 2011 April), the radio pulse precedes the main gamma-ray pulse by about 15–40 per cent of the period (Abdo et al. 2010). This is consistent with the radio emission being associated with the polar cap, and the high-energy emission being associated with a region further out along the open field lines. Still, seven pulsars (the Crab and another six out of 20 known

*E-mail: constantinos.kalapotharakos@nasa.gov (CK);
icontop@academyofathens.gr (IC); demos.kazanas@nasa.gov (DK)

millisecond gamma-ray pulsars) do not follow this simple picture. In these, the radio and high-energy peaks are in phase. This suggests that, at least in these seven pulsars, radio emission is associated with the extended outer magnetosphere. Interestingly enough, in the case of the Crab pulsar, a radio component associated with the polar cap emission region has also been observed, albeit only at low frequencies (Moffett & Hankins 1996). This may further suggest that, at least under certain circumstances, radio emission may be coming both from the polar cap and the outer magnetosphere.

This issue as well as the general stability of the magnetosphere at larger distances motivates a study of its structure at larger radii. Furthermore, a theoretical model that purports to account for the origin of radio emission in the outer magnetosphere was first proposed by Ardavan (1998) (see also Ardavan et al. 2008). Ardavan proposed that a superluminally corotating pattern of electric charges and currents generates at large distances regions of enhanced electromagnetic radiation in vacuum where the local Poynting flux drops as the inverse (and not the inverse square) of the distance from the source. We were particularly intrigued by this proposition and decided to investigate its implications in the pulsar magnetosphere through extensive numerical simulations that probe its structure well outside the light cylinder. As we will see, our results, although still not 100 per cent conclusive, do not seem to support the Ardavan model.

The study of the outer magnetosphere (up to $10r_{lc}$; r_{lc} is the light cylinder radius) requires, on one hand high, enough resolution simulations in order to guarantee minimal numerical dissipation and, on the other hand, the introduction of some (small) amount of diffusivity in order to reduce noise and stabilize the numerical scheme. These simulations exhibit a stable and well-defined undulating smooth current sheet tending towards the split monopole solution (Bogovalov 1999). However, the non-diffusive simulations exhibit a destabilizing spiral region at the crossing of two zero-charge (null) surfaces that happen also to be located on the current sheet. This destabilizing behaviour is enhanced in simulations of increased resolution suggesting a physical (and not numerical) instability.

This paper is structured as follows. In Section 2 we discuss our numerical procedure in comparison with previous treatments of the problem. In Section 3 we present the pulsar antenna radiation pattern. Finally, our conclusions are summarized in Section 4.

2 NUMERICAL SIMULATIONS

2.1 Procedure

The 3D force-free structure of the pulsar magnetosphere in ideal magnetohydrodynamics has been investigated numerically only very recently by two groups (Contopoulos & Kalapotharakos 2010, hereafter CK10, and Bai & Spitkovsky 2010). Both investigations have been based on the formalism of force-free electrodynamics (FFE; Gruzinov 1999; Blandford 2002) and on the numerical procedure described by Spitkovsky (2006). The two investigations differ in the outer boundary conditions of the computational grid. CK10 implemented a perfectly matched layer (PML) that guarantees absorption/non-reflection of the waves reaching the edge of the computational domain. This allowed them to run their original 3D pulsar magnetosphere simulation in a small computational box extending out to only about 2.5 light cylinder radii from the ‘star’ for as long as necessary to achieve steady state. On the other hand, Spitkovsky (2006) and Bai & Spitkovsky (2010) did not implement any special outer boundary condition but simply used a much larger computational domain; as such, they followed the evolution

of the pulsar magnetosphere in the inner two light cylinder radii, for only about two stellar rotations (i.e. until the waves reflected at the boundary reach the distance of two light cylinder radii). Both investigations reached a very similar steady-state magnetospheric configuration.

The issues raised in Section 1 suggest the need for computing the structure of the magnetosphere on a more extended domain than employed so far. Obviously, the implementation of a PML makes our code more suitable to address this problem with the same amount of computational resources than any other FFE numerical code currently available (see CK10, for details about the code). We have run simulations extending out to 10 light cylinder radii in all directions for various pulsar inclination angles. Each simulation required about 35 h on a 1000-core supercomputer. We start off with an inclined magnetostatic dipole field at the centre of our Cartesian computational cube. At time $t = 0$, we set the central dipole in steady rotation. We run the simulation for about two stellar rotations, which is the time needed for the initial transient wave to reach the outer boundary of the numerical grid plus another two rotations to safely reach steady state across our computational grid. The resolution of the simulation is 50 grid points per light cylinder radius, i.e. two times higher than that in CK10 (for a total of 1000^3 grid cells – not taking into account those of the PML). We would like to note here that, in distinction to our original smaller scale simulations that reached only out to $2.5r_{lc}$, our present extended ones include artificial diffusion. This was required in order to better approach the final steady state (we will return to this important point in Section 2.3 and at the end of Section 3). More specifically, we added artificial numerical diffusion terms in the time-dependent Maxwell equations :

$$\frac{1}{c} \frac{\partial \mathbf{B}}{\partial t} = -\nabla \times \mathbf{E} + \eta r_{lc} \nabla^2 \mathbf{B}, \quad (1)$$

$$\frac{1}{c} \frac{\partial \mathbf{E}}{\partial t} = \nabla \times \mathbf{B} - \frac{4\pi}{c} \mathbf{J} + \eta r_{lc} \nabla^2 \mathbf{E}, \quad (2)$$

where η is a dimensionless diffusion parameter acting mostly in the outer magnetosphere beyond $1.5r_{lc}$. The value of η is weighted with $|\nabla^2 \mathbf{B}|$ and $|\nabla^2 \mathbf{E}|$, and its minimum and maximum values throughout the numerical grid are 2×10^{-4} and 6×10^{-3} , respectively.

2.2 Results

Our results are summarized in Fig. 1, where we plot various physical quantities on the poloidal (μ, Ω) plane (i.e. the plane that contains both the rotation and magnetic axes) in steady state for various pulsar inclination angles. These plots were obtained after about three to four stellar rotations, beyond which an almost steady pattern of currents and fields that corotates with the central star is established. Note that in Fig. 1 we have considered the mean values of all the plotted quantities over one period in order to reduce significantly the noise level. On the left, we plot the distribution of meridional electric current density multiplied by r^2 (colour plot) and direction (arrows), and on the right the electric charge density multiplied also by r^2 (colour plot) and meridional magnetic field direction (arrows). The black lines in the right-hand column denote the zero-charge lines. The inclination angles are 15° , 30° , 60° and 90° from top to bottom, respectively. Note that, in FFE, when a corotating steady state is reached, the poloidal electric current and magnetic field components should be parallel everywhere. We do acknowledge that this condition is satisfied to a high degree in our simulations,

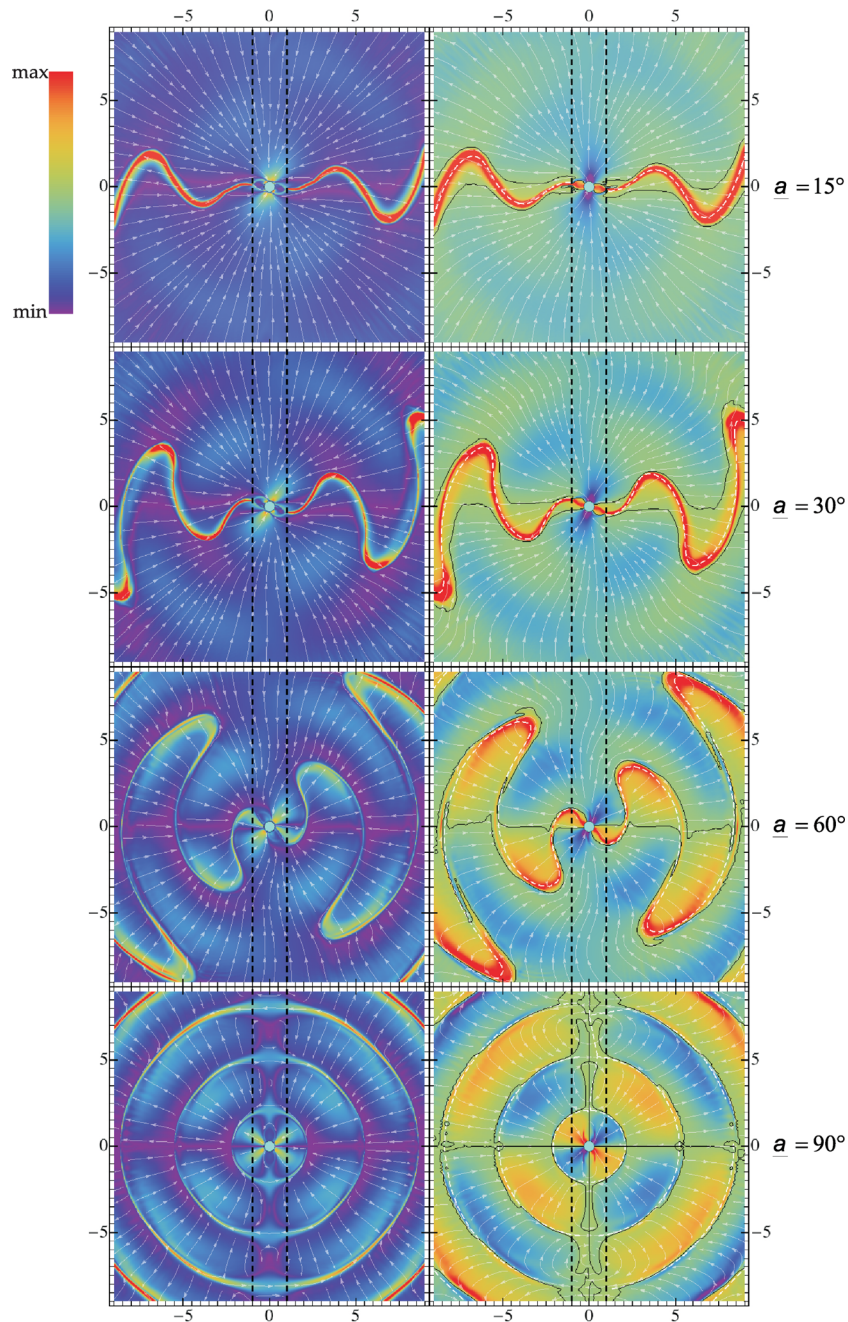


Figure 1. Meridional cross-section of the magnetosphere on the poloidal (μ , Ω) plane in steady state for various pulsar inclination angles. Left-hand panels: meridional electric current density multiplied by r^2 (colour plot) and direction (arrows). Right-hand panels: electric charge density multiplied by r^2 (colour plot) and meridional magnetic field direction (arrows). Inclination angles from top to bottom: 15° , 30° , 60° , 90° . We have considered the mean values of all the plotted quantities over one period in order to reduce the noise level. Light cylinder shown with black vertical dashed lines. The black solid lines and the white dashed lines in the right-hand column indicate the zero-charge lines and the corresponding section of the original ‘Bogovalov’ type current sheet, respectively.

but obviously not 100 per cent. The situation was much worse in our lower resolution – 25 grid points per light cylinder radius – simulations. We offer some idea about the cause of this effect at the end of Section 3.

The most noticeable element of our solution is that an undulating equatorial current sheet forms as predicted by Bogovalov (1999, hereafter B99). This is the 3D generalization of the equatorial current sheet discovered in the axisymmetric investigation of Contopoulos et al. (1999). The white dashed lines in the right-hand

column of Fig. 1 indicate the section of the original ‘Bogovalov’ type current sheet on the (μ , Ω) plane. The current sheet survives as far as the outer boundaries of our numerical simulation for several stellar rotations and is not destroyed by instabilities or reconnection (see however also Sections 2.3 and 3). It originates at the positions where the closed line region ‘touches’ the light cylinder. The current density at those positions is clearly non-uniform. The opening half-angle of the current sheet above and below the rotational equator is about equal to the pulsar inclination angle, as predicted by B99.

2.3 Numerical or physical instabilities?

CK10 and Bai & Spitkovsky (2010) have already identified regions of enhanced electric charge density double layers (positive and negative) described as ‘knots’ just outside the light cylinder. Obviously, the electric field is greatly enhanced between such layers. The results presented in CK10 did not include any artificial diffusivity. In the present study, we realized that this behaviour is more prominent in higher resolution non-diffusive simulations. In Fig. 2 we plot details of the electric charge density distribution in the poloidal plane (μ, Ω) corresponding to $a = 30^\circ$ as obtained in the low (Fig. 2a) and high (Fig. 2b) resolution non-diffusive simulations, and in the high-resolution simulation with artificial numerical diffusivity (Fig. 2c). In Fig. 2(a) we observe that the region of strong positive and negative electric charges is smoother than in Fig. 2(b). As a general trend, in higher resolutions numerical instabilities tend to be suppressed, whereas physical instabilities tend to manifest themselves. The fact that the feature observed in Fig. 2(a) is enhanced in simulations of increased resolution signifies an instability of physical rather than numerical underpinnings. Nevertheless, we cannot yet rule out that it may also be due to some kind of numerical instability. In Fig. 2(c) we see that the introduction of the diffusion term in equations (1) and (2) clearly smooths out this feature.

We realized that such ‘knots’ appear where two different zero-charge surfaces cross each other *on* the current sheet. In Fig. 2, the sign of the charge density on the poloidal plane reveals this strange topology: the crossing of two zero-charge (null) surfaces creates an X-point on the current sheet. Above and below this point along the current sheet double layers of opposite electric charges are formed. We have also found that dissipative solutions of the magnetosphere above and below this point exhibit electric field components parallel and antiparallel to the magnetic field, respectively.

The question with this feature is whether it represents a real structure or an artefact of our numerical scheme. Is this feature introduced by the non-diffusive scheme (Fig. 2a, b) or is it that the diffusion introduced in producing Fig. 2(c) smooths out a really singular feature of the solution? The fact that two independent nu-

merical schemes (Bai & Spitkovsky 2010; CK10) exhibit similar behaviour and that this is a rather extraordinary region (the confluence of two zero-charge surfaces on a current sheet) supports the view that this may indeed be a real feature.

3 THE PULSAR ANTENNA RADIATION PATTERN

Overall, the magnetic field assumes an open split-monopole-like structure that corresponds to the radiation field of an antenna with E almost perpendicular to B , and both E and B dropping like $1/r$ on average with distance from the central antenna (in our case, the rotating central dipole). We remind the reader that in any radiation pattern, a characteristic distance exists that separates the inner from the outer radiation field region, the so-called Fresnel distance defined as

$$r_{\text{Fresnel}} \equiv l^2/\lambda \sim r_{\text{lc}}. \quad (3)$$

Here, $r_{\text{lc}} \equiv cP/(2\pi)$ is the light cylinder radius, $l \sim 2r_{\text{lc}}$ is the linear extent of the ‘pulsar antenna’, and $\lambda = 2\pi r_{\text{lc}}$ is the wavelength of the radiation as seen in the electromagnetic field patterns of Fig. 1. Our simulation box extends beyond a few times the above distance, and therefore it is suitable to study the pulsar antenna far-field radiation pattern.

While the Poynting flux of the rotating magnetosphere averaged over the entire 4π solid angle decreases as $\sim 1/r^2$, as expected from the conservation of electromagnetic radiation, this flux is not distributed uniformly over the sphere. In Fig. 3, we plot the Poynting flux distribution on the Mollweide (elliptical) projection of a sphere of radius $r = 8 r_{\text{lc}}$ centred on the central star ($\theta = 0^\circ$ along the axis of rotation). One sees that the Poynting flux displays local maxima. Obviously, in steady state, the radiation pattern should corotate with the star. For $a = 90^\circ$ the 50 per cent of the Poynting flux (black dotted curve of Fig. 3) is emitted from only 0.6π sr.

Ardavan (1998) proposed that singular electromagnetic radiation features take place in vacuum when a pattern of electric charges

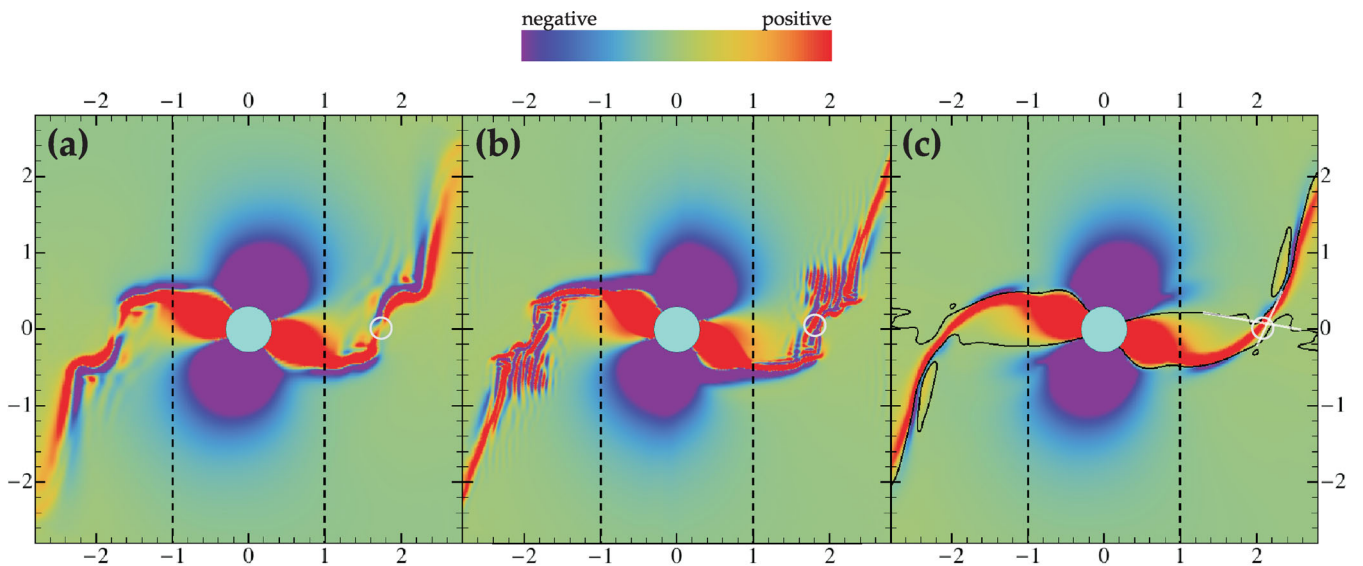


Figure 2. Detail of the electric charge density in the poloidal (μ, Ω) plane in steady state for an inclination angle of 30° . Panel (a): low-resolution (25 grid points per light cylinder radius) non-diffusive simulation. Panel (b): high-resolution (50 grid points per light cylinder radius) non-diffusive simulation. Panel (c): high-resolution (50 grid points per light cylinder radius) simulation with artificial diffusion as in equations (1) and (2). Zero-charge (null) surfaces shown with solid black lines. Crossing of null surfaces shown with white line elements and circle. Light cylinder shown with dashed lines.

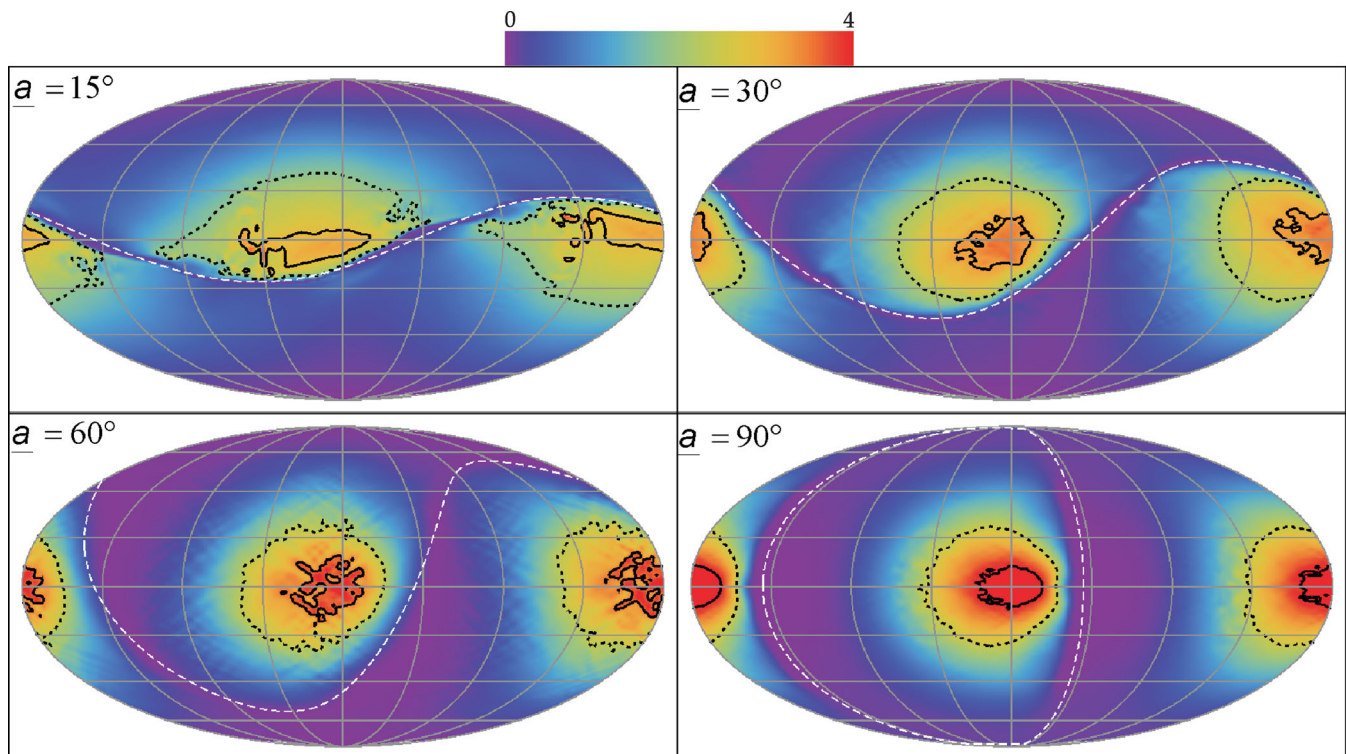


Figure 3. Distribution of the Poynting flux in Mollweide (elliptical) projection of the sphere $r = 8 r_{lc}$ centred on the central star for the inclination angles indicated in the panels. The linear colour scale ranges from zero up to four times the corresponding mean Poynting flux value. The highest 50 per cent of the values are contained inside the dashed black lines, and the highest 10 per cent inside the solid black lines. The maximum of the Poynting flux forms a spiral pattern near the (rotational) equator. Note that the 50 per cent of the Poynting flux in $a = 90^\circ$ case (dotted curve) is emitted only through 15 per cent of the entire 4π solid angle. The same area corresponding to the $a = 15^\circ$ case is 40 per cent larger. The white dashed lines trace the locus of the current sheet.

and currents corotates superluminally (only the pattern corotates; nothing is moving superluminally). In Section 1, we acknowledged that this was one of our original motivations for extending the simulations of CK10 to much larger distances. Preliminary results hinted that the local Poynting flux in regions of enhanced electromagnetic field discussed in Section 2.3 drops as $1/r$ (and *not* as $1/r^2$) with distance r , as anticipated in vacuum by Ardavan (1998). This was very encouraging! However, the fact that certain features of the simulation were noisy and not consistent with steady state led us to increase the spatial resolution by a factor of 2 and to introduce diffusivity in order to stabilize the numerical scheme. As a consequence, any singular electromagnetic radiation feature was killed.

Unfortunately, we are still not in a position to completely dismiss the possibility that the physical solution includes regions of enhanced electromagnetic field (radiation caustics?) and that the introduction of (albeit small) diffusion does not artificially suppress their development. Furthermore, diffusivity introduces also a gradual decrease of E with distance below its theoretical steady-state corotation value $(r \sin \theta / r_{lc}) B_p$, and therefore magnetic field lines gradually loose corotation with the central star. This manifests itself in Fig. 1 through the inability of our numerical procedure to satisfy 100 per cent the steady-state requirement that the poloidal components of the electric current and the magnetic field must be parallel everywhere.

4 CONCLUSIONS

In this paper, we presented the results of extensive numerical simulations of the 3D force-free ideal pulsar magnetosphere out to a

distance of about 10 times the light cylinder radius. Our results clearly show that the undulating equatorial current sheet survives over that distance and over several stellar rotations, implying that it represents an almost steady feature of the magnetosphere. The introduction of a small artificial diffusivity was necessary for the stabilization of the numerical scheme. Using this scheme the current sheet appears smooth and very similar to the one given analytically in B99. Overall, it is primarily charged positively (negatively) for an aligned (counter-aligned) rotator.¹

Interestingly enough, the regions of strong charge density first seen in CK10 are enhanced in higher resolution non-diffusive simulations. These regions are formed near the locus of the crossing of two zero-charge surfaces. A destabilizing behaviour more prominent in high-resolution simulations is observed around these regions. Nevertheless, this behaviour is suppressed after the introduction of artificial diffusivity (necessary for the stabilization of the numerical scheme), thus raising questions about its true nature (physical or numerical).

We present also the pulsar antenna spiral (for oblique rotators) radiation pattern. The Poynting flux is not uniformly distributed over the entire sphere. Its maximum is along a spiral direction near the (rotational) equator. The Poynting flux corresponding to the smooth high-resolution solutions produced by the diffusive simulations drops everywhere as r^{-2} , implying that enhanced electromagnetic fields similar to those proposed by Ardavan (1998) are not present. Their existence, however, cannot yet be conclusively ruled

¹ Obviously, the concept of alignment gradually loses its meaning as we approach 90° inclination angles.

out since such effects are expected to be sensitive to diffusivity. Further investigation with much higher resolution is required.

ACKNOWLEDGMENTS

We would like to acknowledge extensive discussions with Houshang Ardavan, as well as with Christos Efthymiopoulos, Avi Loeb, Maxim Lyutikov, Cole Miller, Ramesh Narayan and Sasha Tchekhovskoy. We thank also the anonymous referee whose suggestions motivated us to develop a novel numerical technique that improved the quality of the presented results.

REFERENCES

- Abdo A. A. et al., 2010, *ApJS*, 187, 460
 Ardavan H., 1998, *Phys. Rev. E*, 58, 6659
 Ardavan H., Ardavan A., Fasel J., Middleditch J., Perez M., Schmidt A., Singleton J., 2008, *Proc. Science*, CRAB2008, 016
 Bai X.-N., Spitkovsky A., 2010, *ApJ*, 715, 1282
 Blandford R. D., 2002, in Gilfanov M., Sunyaev R., Churazov E., eds, *Lighthouses of the Universe*. Springer, Berlin
- Bogovalov S., 1999, *A&A*, 349, 1017 (B99)
 Contopoulos I., 2005, *A&A*, 442, 579
 Contopoulos I., Kalapotharakos C., 2010, *MNRAS*, 404, 767 (CK10)
 Contopoulos I., Kazanas D., Fendt C., 1999, *ApJ*, 511, 351
 Gruzinov A., 1999 (arXiv:astro-ph/9902288)
 Gruzinov A., 2005, *Phys. Rev. Lett.*, 94, 021101
 Guillemot L., Cognard I., Johnson T. J., Venter C., Harding A. K., 2011, in Burgay M., D’Amico N., Esposito P., Pellizzoni A., Possenti A., eds, *AIP Conf. Ser. 1357, Multiwavelength Analysis of Four Millisecond Pulsars*. Am. Inst. Phys., New York, p. 241
 Harding A. K., Stern J. V., Dyks J., Frackowiak M., 2008, *ApJ*, 680, 1378
 Kalapotharakos C., Contopoulos I., 2009, *A&A*, 496, 495
 Lyubarsky Y. E., 1996, *A&A*, 311, 172
 Moffett D. A., Hankins T. H., 1996, *ApJ*, 468, 779
 Muslimov A. G., Harding A. K., 2004, *ApJ*, 606, 1143
 Pétri J., Kirk J. G., 2005, *ApJ*, 627, L37
 Ransom S. M. et al., 2011, *ApJ*, 727, L16
 Spitkovsky A., 2006, *ApJ*, 648, L51
 Timokhin A. N., 2006, *MNRAS*, 368, 1055

This paper has been typeset from a $\text{\TeX}/\text{\LaTeX}$ file prepared by the author.